International Journal of GEOMATE, May 2019, Vol.16, Issue 57, pp.209 - 216
Geotec., Const. Mat. & Env., DOI: https://doi.org/10.21660/2019.57.70809
ISSN: 2186-2982 (Print), 2186-2990 (Online), Japan

APPLICATION OF NUMERICAL FILTER TO A TAYLOR GALERKIN FINITE ELEMENT MODEL FOR MOVABLE BED DAM BREAK FLOWS

*Dhemi Harlan[1], Mohammad Bagus Adityawan[1], Dantje Kardana Natakusumah[2], Nur Lely Hardianti Zendrato[2]

[1]Water Resources Engineering and Management, Institut Teknologi Bandung, Jatinangor, Indonesia
[2]River and Sedimentation Laboratory, Institut Teknologi Bandung, Jatinangor, Indonesia

*Corresponding Author, Received: 13 Dec. 2018, Revised: 31 Dec. 2018, Accepted: 15 Jan. 2019

ABSTRACT: The dam break-induced propagation over a movable bed has given strong interest in numerical modeling. The shock wave, generally found in the wavefront, is a challenge in numerical modeling since this condition often leads to numerical instability. Additionally, the scouring beneath the wave requires coupling of hydraulic and sediment transport models. The objective of this research is to develop a one-dimensional model based on a finite element method to simulate an experimental case of a dam break-induced flow and the bed scouring beneath it. The two-step Taylor Galerkin scheme is used to solve the governing equations. In addition, Hansen numerical filter is used to handle shock wave and to increase the numerical stability of the developed model. The results show good agreement to the experimental data. Additionally, the applied numerical filter is able to reduce oscillation and improve the stability of the model.

Keywords: Dam break flow, Movable bed, Taylor Galerkin scheme, Numerical instability, Hansen filter

1. INTRODUCTION

Dam failure is normally caused by several factors, they could be by geotechnical failure, the strength of construction, excess pore water pressure, quality of material used for construction, error in construction planning, natural disasters (earthquake, erosion), and other. The dam failure will directly effects scouring downstream of the dam. Scouring occurs when the erosion capacity due to dam break flows exceeds the capacity that can be accommodated. Meanwhile, this will indirectly disrupt clean water supply, electricity supply, damage homes and infrastructures, and cause environmental damage. The devastating effect of a dam break to its downstream area due to the failure of Wai Ela natural dam has been shown in [1]. In recent years, dams are required to provide a mitigation plan in the case of failure. Therefore, numerical models are of significant importance in estimating the effect of a dam break flow.

A dam break simulation is commonly approach using the shallow water equation. The equation can be numerically solved using the finite difference method (FDM), finite volume method (FVM), or finite element method (FEM). FDM is one of the most common methods for modeling as described in [2]. However, they are less flexible and have a tendency to give numerical instability. A numerical study of a hypothetical one-dimensional dam break using several FDM schemes was conducted as in [3]. The results showed that the shock wave is significantly causing numerical oscillation, especially for lower order schemes. Thus, a numerical filter such as Total Variation Diminishing (TVD) is highly required.

FVM provides faster computation. A model based on the one-dimensional shallow water equation, solved using an FVM scheme was developed, as in [4]. The model required an artificial dissipation using a weighting factor to handle abrupt changes of the flow. Adityawan et.al.[5] used an FVM scheme with a slope limiter to simulate an experimental case of a dam break flow. The slope limiter acts as an artificial dissipation to handle shock wave. The model was improved and it showed the importance of bed stress under the front wave in relation to scouring, as in [6]. They coupled the shallow water equation with k-ω a model for a better bed stress assessment.

In a real event of a dam break, the model domain may be highly irregular. In this case, FEM provides a more flexible way to calculate points within a computational domain. The effective use of FEM in global modeling was shown in [7]. A model for flooding in the coastal area based on the Shallow Water Equation, solved using FEM was developed in [8]. The model is able to handle the wet/dry condition. However, there are no artificial dissipation or numerical filter for shock capturing. A Galerkin FEM with a characteristic method to absorb shock wave was employed in [9]. Nevertheless, the application of a numerical filter or artificial dissipation is favorable due to its

simplicity.

Spinewise and Capart [10] investigated the velocity profile and sediment grain concentration by laboratory experiment by further developing the setup, as in [11]. They used a longer flume and improved the process of withdrawing the gate. The gate is opened faster than in the previous, resulting in a more upright initial water level condition. In addition, they developed a shallow water theory that is appropriate with the level of detailed that was achieved in the experiment. The numerical approach [12] and the analytical approach [13] were selected, as in [10], in order to capture the significant influence of frictional momentum losses on the development of the wave front.

In this research, Taylor Galerkin finite element scheme, firstly developed by Donea [14], is used as a numerical scheme. The scheme presented here was the variant scheme developed [15] originally for the aerodynamic application. Then, it was extended to shallow water problems in [16,17]. The model has been tested and compared to an FDM scheme to simulate a dam break flow on a fixed bed [18]. It showed that the FEM performs better than the FDM. In this paper, the scheme is developed for the simulation of movable bed dam-break flows. The solutions of Taylor Galerkin model are compared to the experimental data in [11] for the different test case. A numerical filter from Hansen [19] is used to handle shock and improve the model stability. The filter has been successfully used in a finite difference model as in [20].

2. GOVERNING EQUATION

The one-dimensional movable bed dam break flows can be expressed by using the continuity equation and momentum equation [10] in the vector form following below.

$$\frac{\partial \tilde{z}}{\partial t} + \frac{\partial q}{\partial x} = 0 \quad \text{..... (1)}$$

$$\frac{\partial z_0 c_0}{\partial t} + \frac{\partial j}{\partial x} = 0 \quad (2)$$

$$\frac{\partial \mu}{\partial t} + \frac{\partial \pi}{\partial x} + \underline{\sigma}\frac{\partial z}{\partial x} = -\tau \quad (3)$$

with

$$q = h\overline{u}, \quad j = h\overline{cu}, \quad \pi = h\overline{\rho u^2} + h\overline{\sigma} \quad (4)$$

$$z_0 = \underline{z} + \frac{h\overline{c}}{c_0}, \quad \mu = h\overline{\rho u} \quad (5)$$

The equations above are general and do not assume certain forms for the velocity and the profiles of concentration. Here, q is the total volumetric discharge, j is granular transport rate, and π is the momentum flux. They are in per unit width. Parameter of z_0 is the bed elevation after all solid grains are settled corresponding to vethe rtical column and μ is the momentum density per unit bed area.

Capart & Fraccarollo (2011) in [10] assumed the equations for vertical profiles of velocity u and concentration c, can be expressed as below.

$$u(z) = \begin{cases} \tilde{u} & \underline{z} + \delta \le z \le \underline{z} + h \\ \tilde{u}(z - \underline{z})/\delta & \underline{z} \le z \le \underline{z} + \delta \\ 0 & z \le \underline{z} \end{cases} \quad (6)$$

$$c(z) \begin{cases} 0 & \underline{z} + \delta < z \le \underline{z} + h \\ \underline{c} + (\tilde{c} - \underline{c})(z - \underline{z})/\delta & \underline{z} < z \le \underline{z} + \delta \\ c_0 & z \le \underline{z} \end{cases} \quad (7)$$

where $\tilde{u}$ is the flow velocity at the free surface, h is the total flow depth, $\underline{z}$ is the bed elevation, δ is the thickness of the bed load, $\tilde{c}$ is the granular concentration at the top of the bed load layer, $\underline{c}$ is the granular concentration at the base of the bed load layer, and c_0 is the granular concentration in the static bed. For the balance variables of $\tilde{z}$, $z_0 c_0$, and μ are given as

$$\tilde{z} = \underline{z} + h \quad (8)$$

$$z_0 c_0 = \underline{z} c_0 + \delta\left(\frac{1}{2}\underline{c} + \frac{1}{2}\tilde{c}\right) \quad (9)$$

$$\mu = \rho_w\left(h - \frac{1}{2}\delta\right)\tilde{u} + (\rho_s - \rho_w)\delta\tilde{u}\left(\frac{1}{6}\underline{c} + \frac{1}{3}\tilde{c}\right) \quad (10)$$

The parameters of ρ_w and ρ_s are the mass densities of the pure water and sediment grains. The flux variables of q, j, π can be given as

$$q = \left(h - \frac{1}{2}\delta\right)\tilde{u} \quad (11)$$

$$j = \delta\tilde{u}\left(\frac{1}{6}\underline{c} + \frac{1}{3}\tilde{c}\right) \quad (12)$$

$$\pi = \rho_w\tilde{u}^2\left(h - \frac{2}{3}\delta\right) + (\rho_s - \rho_w)\delta\tilde{u}^2\left(\frac{1}{12}\underline{c} + \frac{1}{4}\tilde{c}\right) + \frac{1}{2}\rho_w g h^2 + (\rho_s - \rho_w)g\delta^2\left(\frac{1}{6}\underline{c} + \frac{1}{3}\tilde{c}\right) \quad (13)$$

The basal normal stress, $\underline{\sigma}$ and the basal shear stress, $\underline{\tau}$ are given as

$$\underline{\sigma} = \rho_w g h + (\rho_s - \rho_w)g\delta\left(\frac{1}{2}\underline{c} + \frac{1}{2}\tilde{c}\right) \quad (14)$$

$$\underline{\tau} = \frac{1}{2}(\underline{c} + \tilde{c})(\rho_s - \rho_w)Rg\delta \quad (15)$$

where $R = \tan\varphi$ is the tangent of the internal angle of friction.

3. NUMERICAL SCHEME

A general form of a one-dimensional movable dam break flows can be written in conservative form as following below

$$\frac{\partial U}{\partial t} + \frac{\partial F}{\partial x} = S \quad (16)$$

Where

$$U = \begin{Bmatrix} \tilde{z} \\ z_0 c_0 \\ \mu \end{Bmatrix}, \quad F = \begin{Bmatrix} q \\ j \\ \pi \end{Bmatrix}, \quad S = \begin{Bmatrix} 0 \\ 0 \\ -\underline{\tau} - \underline{\sigma}\frac{\partial z}{\partial x} \end{Bmatrix} \quad (17)$$

The numerical scheme used to discretize the equations above is two steps Taylor Galerkin FEM scheme. This scheme is analog to two-step Lax-Wendroff scheme based on FDM.

3.1 Time Discretization

The numerical algorithm used here is by using second order of Taylor Series to develop U in time of $t = t^n$ as follow.

$$U^{n+1} = U^n + \Delta t\left(\frac{\partial U}{\partial t}\right)^n + \frac{\Delta t^2}{2}\left(\frac{\partial^2 U}{\partial t^2}\right)^n \quad (18)$$

Rearranging Equation (16), so the derivative of time as the derivative of space following below

$$\frac{\partial U}{\partial t} = S - \frac{\partial F}{\partial x} \quad (19)$$

For the second order,

$$\frac{\partial^2 U}{\partial t^2} = \frac{\partial}{\partial t}\left(S - \frac{\partial F}{\partial x}\right) = \frac{\partial S}{\partial U}\frac{\partial U}{\partial t} - \frac{\partial}{\partial x}\frac{\partial F}{\partial U}\frac{\partial U}{\partial t}$$
$$= G\left(S - \frac{\partial F}{\partial x}\right) - \frac{\partial}{\partial x}\left(A\left(S - \frac{\partial F}{\partial x}\right)\right) \quad (20)$$

By substituting (19) and (20) to (18) then

$$U^{n+1} = U^n + \Delta t\left(S - \frac{\partial F}{\partial x}\right)^n + \frac{\Delta t^2}{2}\left(G\left(S - \frac{\partial F}{\partial x}\right) - \frac{\partial}{\partial x}\left(A\left(S - \frac{\partial F}{\partial x}\right)\right)\right)^n \quad (21)$$

3.2 Space Discretization

In space discretization, several functions are used here for an approximation as below:

$$U = U^i N_i, \quad F = F^i N_i, \quad S = S^i N_i \quad (22)$$

Where N_i is the piecewise linear shape function for nodal *i*, and

$$G = G^e P_e, \; A = A^e P_e, \quad (23)$$

Where P_e weight residual is the piecewise constant shape function for elemen e . By using weight residual process to equation (21) by shthe ape function $\boldsymbol{N_i}$, the equation will be

$$\int_\Omega (U^{n+1} - U^n)N_i d\Omega = \Delta t \int_\Omega \left(S - \frac{\partial F}{\partial x}\right)^n N_i d\Omega + \frac{\Delta t^2}{2}\int_\Omega \left(G\left(S - \frac{\partial F}{\partial x}\right) - \frac{\partial}{\partial x}\left(A\left(S\frac{\partial F}{\partial x}\right)\right)\right)^n N_i d\Omega \quad (24)$$

where Ω is the space domain, and a consistent mass matrix is given as

$$M = \int_\Omega N_i N_j d\Omega \quad (25)$$

By using Gauss theorem to get the weak form, then multiply both sides of equation (24) by N_j and using equation (25), the equation is transformed into the below

$$(M\Delta U) = \Delta t \int_\Omega \left[\left(S - \frac{\partial F}{\partial x}\right)^n N_i\right] N_j d\Omega + \frac{\Delta t^2}{2}\int_\Omega \left(G\left(S - \frac{\partial F}{\partial x}\right) - \frac{\partial}{\partial x}\left(A\left(S - \frac{\partial F}{\partial x}\right)\right)\right)^n N_i d\Omega \quad (26)$$

The algorithm above can be applied for a set of equation systems. The problems appear when the system involves the evaluation and the multiplication of matrix A and G. This process consumes computer resources. Therefore, equation (26) is arranged using two steps algorithm as given in [16].

The numerical algorithm used here is by using second order of Taylor Series to develop U in time of $t = t^n$ as follow.

$$(M\Delta U) = \Delta t \left\{ \int_\Omega \left\{ \left[S_i^n N_i + \left(S^{n+\frac{1}{2}} - \bar{S}^n \right) \right] N_j + \left[F_k^{n+\frac{1}{2}} - \overline{F_k}^n + F_i^{k^n} N_i \right] \frac{\partial N_j}{\partial x_k} d\Omega \right\} + \int_\Gamma -F_{in} N_i^n - \left[F^{n+1/2} - \bar{F}^n \right] N_j d\Gamma \right\} \quad (27)$$

3.3 Numerical Filter

Taylor Galerkin model as a finite element method is capable to employ flexible grid. However, it has been shown in [16,17,18] that Taylor Galerkin is prone to oscillation and instability especially in handling the shock. The developed model employs a numerical filter to handle shock wave as proposed in [19]. The filter is used for each time step at each computational point. The values of water depth and velocity are updated at each iteration using the following equation.

$$F(i)=C\times F(i)+0.5(1-C)(F(i-1)+F(i+1)) \quad (28)$$

The filter can be further derived for second order equation as follow.

$$F(i) = C \times F(i) + \frac{2}{3}(1 - C)\frac{[F(i+1) + F(i-1)]}{2} + \frac{1}{3}(1 - C)\frac{[F(i+2) + F(i-2)]}{2} \quad (29)$$

C value is given as 0.99, with F corresponds to the filtered parameters.

4. TEST CASES DESCRIPTION

The developed model is applied to simulate an experimental case of a dam break flow with movable bed [11]. The experiment was conducted in a laboratory with PVC (Particle Tracking Velocimetry) grains.

The dam break was simulated in a flume of 6 m length, 25 cm width, and 70 cm height. A gate is located at the middle of the flume. The flume is filled with water at one side of the gate. The bed is formed by a layer of initially motionless sediment. The gate is opened suddenly, releasing the water. The flow velocity and the transported sediment were then measured. Coarse, lightweight PVC grains are used in the experiments. The particles are white in color, cylindrical in shape with an approximately equal height and base diameter, and an equivalent spherical diameter D = 3.9 mm, measured from the bulk volume of 1000 particles. The grains have a density $\rho_s = 1580\ kg\ m^{-3}$ and friction angle $\varphi = 38^0$, as estimated from critical repose angle of dry grthe anular heap. They are poured in place at loose packing to produce a bed of granular concentration $c_0 \approx 0.58$. The detail of the laboratory experiment can be found in [11].

The initial conditions for both layers of water and water-saturated grains are at rest on both sides of the gate. The vertical gate is positioned at x = 0. The initial conditions at t = 0 are given by

$$\underline{z}(x,0) = \begin{cases} \underline{z}_L, & x < 0, \\ \underline{z}_R, & x > 0, \end{cases} \quad (30)$$

$$\tilde{z}(x,0) = \begin{cases} \tilde{z}_L, & x < 0, \\ \tilde{z}_R, & x > 0, \end{cases} \quad (31)$$

$$\tilde{u}(x,0) = 0 \quad (32)$$

The bed and the free surface are initially horizontal on both sides of the gate, but levels $\underline{z}_L$, $\underline{z}_R$, $\tilde{z}_L$, $\tilde{z}_R$ on the left and right sides will be in two cases is given in Table 1 below.

Table 1 Test cases data for simulation

Case	Material	$\underline{z}_L$ (m)	$\tilde{z}_L$ (m)	$\underline{z}_R$ (m)	$\tilde{z}_R$ (m)
1	PVC	0	0.35	0.0	0.01
2	PVC	0.05	0.35	0.0	0.01

The illustration of test cases for the initial condition on Table 1 can be shown in Fig. 1 and Fig. 2 below.

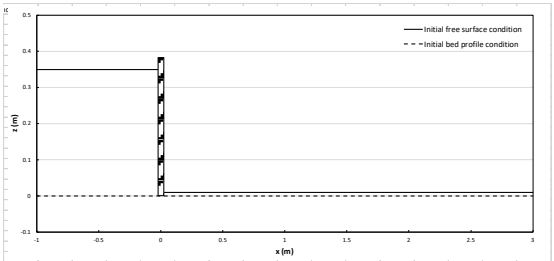

Fig. 1. The initial condition of case 1 at t = 0

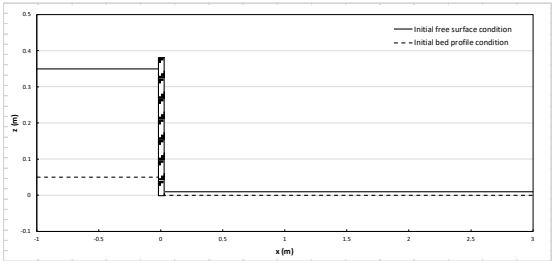

Fig. 2. The initial condition of case 2 at t = 0

The length of the domain in the numerical simulation is extended to 10 meters. This is to ensure that the model is not affected by the

boundary conditions. The number of elements and nodes are 500 elements and 501 nodes with a spacing of 0.02 meter.

5. RESULTS AND DISCUSSION

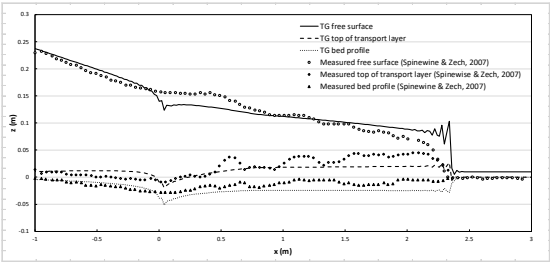

Fig. 3. Comparison of the free surface, top of the transport layer, and bed profile between Taylor Galerkin simulation and experimental data
(case 1: $\underline{z}_L = 0$, $\tilde{z}_L = 0.35$, $\underline{z}_R = 0$, $\tilde{z}_R = 0.01$)

Figures 3 and 4 show the comparison of the simulation results from the developed model (without the numerical filter) to the experimental data for case 1 and case 2, respectively. Here, the bed profile can be identified as $\underline{z}$, the top of the bed layer as $\underline{z} + \delta$, and the free surface as $\tilde{z} = \underline{z} + h$.

Figure 3 shows the free surface, top layer, and bed layer profiles at t = 1.25 second for case 3. The calculated free surface at the gate and at the wave front shows high oscillation due to the abrupt changes of the flow hydraulic conditions. The free surface suddenly drop around the gate ($\tilde{z} = 0.125$) followed by a milder slope to the wave front. Numerical instability begins to appear on x = 2.1 meter until x = 2.3 meter with $\tilde{z} = 0.07$ then down suddenly to close to bed profile with $\tilde{z} = 0.01$, respectively.

The calculated top layer profile in figure 1 is shown to have a good comparison to the experimental data. Nevertheless, oscillation occurs around the dam position with $\underline{z} + \delta = -0.02$. The bed profile gives an increasing trend from the gate to x = 0.7 meter, then relatively constant to x = 2.2 meter with $\underline{z} + \delta = 0.02$. Oscillation appears at x = 2.2 meter to x = 2.3 meter due to the same reason.

The calculated bed profile in Figure 3 also shows a good comparison to the experimental data. Similar trends to the top layer and the free surface profiles are observed. A downward trend around the gate with oscillation with $\underline{z} = -0.05$. An upward trend to x = 0.7 meter, then relative constant to x = 2.2 meter with $\underline{z} = -0.025$. Oscillation also starts to appear at x = 2.2 until x = 2.3 meter and up suddenly to $\underline{z} = 0$.

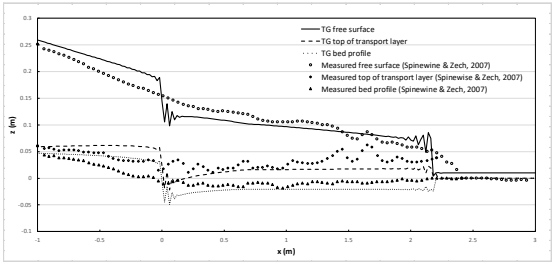

Fig. 4. Comparison of the free surface, top of the transport layer, and bed profile between Taylor Galerkin simulation an d experimental data
(case 2: $\underline{z}_L = 0.05$, $\tilde{z}_L = 0.35$, $\underline{z}_R = 0.01$, $\tilde{z}_R = 0.01$)

Figure 4 shows the free surface profile, top layer, and bed layer profiles at t = 1.25 second for case 2. In general, the trends are the same as in case 1. However, oscillation due to numerical stability, in this case, is stronger, especially around the gate.

The calculated free surface shows a steeper gradient than the measured value around the dam position at the center of coordinates with $\tilde{z} = 0.11$. A strong oscillation is also observed in this location. The calculated profiles after this location shows a good comparison to the measure value until the wave front at x = 2.0 meter. Here, numerical instability appears on until x = 2.2 meter with $\tilde{z} = 0.06$ then drop suddenly to $\tilde{z} = 0.01$.

The calculated top layer profile also shows similar trends to the measured data. A sudden elevation drop is observed around the dam position with $\underline{z} + \delta = -0.01$ and then start slightly increasing to x = 0.7 meter, then relative constant to x = 2.2 meter with $\underline{z} + \delta = 0.02$. Nevertheless, oscillation occurs at the similar locations to the free surface profile, around the gate and at the wave front.

The calculated bed profile shows a good comparison to the experimental data. Similar trends to the top layer profile are observed. The elevation drop suddenly around the dam position with $\underline{z} = -0.04$ and then start slightly ascending to x = 0.7 meter, then relative constant to x = 2.2 meter with $\underline{z} = -0.02$. At x = 2.2 meter starts the numerical instability until x = 2.3 meter and up suddenly to $\underline{z} = 0$.

Figures 5 and 6 show the simulation result of the developed model (with numerical filter) and the experimental data for case 1 and case 2, respectively. The bed profile can be identified as $\underline{z}$, the top of the bed layer as $\underline{z} + \delta$, and the free surface as $\tilde{z} = \underline{z} + h$, as in Figures 3 and 4.

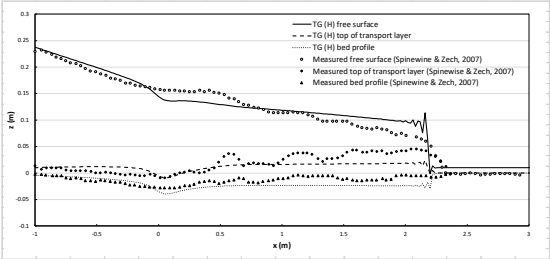

Fig. 5. Comparison of the free surface, the top of the transport layer, and bed profile between Taylor Galerkin (Hansen filter) simulation and experimental data (case 1: $\underline{z}_L = 0$, $\tilde{z}_L = 0.35$, $\underline{z}_R = 0$, $\tilde{z}_R = 0.01$)

Figure 5 shows the free surface profile, top layer, and bed layer profiles at t = 1.25 second for case 1. Overall, oscillation is reduced significantly due to the application of the numerical filter. However, the oscillation at the wavefront sill appears. The calculated free surface drops around the gate due to its sudden opening with $\tilde{z} = 0.135$. At this location, the numerical filter significantly improves the stability of the model. The surface profile shows a downward trend from the gate to x = 2.1 meter. At the wave front, oscillation appears on x = 2.0 meter until x = 2.2 meter with $\tilde{z} = 0.08$. The surface profiled drop suddenly approaching the bed level with $\tilde{z} = 0.01$. The estimated wave front location is behind the experiment data.

The calculated top layer profile also shows a sudden drop around the gate with $\underline{z} + \delta = -0.01$. The top layer slowly increases to x = 0.7 meter, then relative constant to x = 2.1 meter with $\underline{z} + \delta = 0.02$. Oscillation still appears around the wave front at x = 2.1 meter until x = 2.2 meter and down suddenly to $\underline{z} + \delta = 0$.

The calculated bed layer profile gives a similar trend to the calculated top layer profile. The profile changes abruptly around the gate with $\underline{z} = -0.04$ and then start slightly ascending to x = 0.7 meter, then relative constant to x = 2.1 meter with $\underline{z} = -0.025$. Again, oscillation appears around the wave front at x = 2.1 meter until x = 2.2 meter

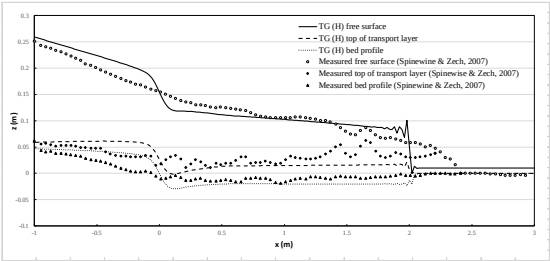

Fig. 6. Comparison of the free surface, top of the transport layer, and bed profile between Taylor Galerkin (Hansen filter) simulation and experimental data (case 1: $\underline{z}_L = 0.05$, $\tilde{z}_L = 0.35$, $\underline{z}_R = 0$, $\tilde{z}_R = 0.01$)

Figure 6 shows the free surface profile, top layer, and bed layer profiles at t = 1.25 second for case 2. The free surface profile shows a significant reduction of the oscillation to that in Figure 6. The surface profile around the gate shows a sudden drop to $\tilde{z} = 0.12$ without any oscillation around x = 0 and then sloping down to the distance of 2.0 meter. However, mild oscillation is still observed around the wave front from x = 1.8 meter until x = 2.1 meter with $\tilde{z} = 0.07$ then suddenly drop to $\tilde{z} = 0.01$, respectively. In addition, the wave front location is considerably behind to that obtains from experiment and model without fila ter.

The calculated top layer profile shows a similar trend to the that from the model without a filter as well as the experimental data. A sudden drop is found around the gate with $\underline{z} + \delta = 0.0$ and then start slightly ascending to x = 0.7 meter, then relative constant to x = 1.9 meter with $\underline{z} + \delta = 0.02$. Oscillation is also found around the wave front from x = 1.9 meter until x= 2.1 meter.

The calculated bed profile shows good agreement to the experimental data. The bed level drops around the gate with $\underline{z} = -0.03$ and then start slightly ascending to x = 0.7 meter, then relative constant to x = 2.2 meter with $\underline{z} = -0.02$. However, as in the free surface and top layer profiles, mild oscillation is observed from x = 1.9 meter until x = 2.1 meter.

The results are further analyzed to evaluate the performance of the numerical filter. Pearson Correlation and Root Mean Square Error (RMSE) are calculated for the free surface profile, top layer profile and bed layer profile, from the model and the experiment data, for all cases. The results are given in Table 2 below

Table 2 Filter Evaluation (Pearson Correlation, RMSE) of Free Surface, Top Layer, and Bed Layer

Model	Free Surface			
	Case 1		Case 2	
	Pearson	RMSE	Pearson	RMSE
Free Surface				
With Filter	0.96	5.16	0.94	6.43
Without Filter	0.94	8.07	0.93	6.62
Top layer				
With Filter	0.47	34.56	0.30	27.68
Without Filter	0.56	27.02	0.30	20.06
Bed layer				
With Filter	0.27	21.32	0.79	15.79
Without Filter	0.26	21.32	0.75	14.74

The numerical filter gives a better prediction of the free surface profile. In both cases, results from the model with filter give a higher correlation and a lower RMSE to the experiment data than those from without filter. However, the estimated value of top and bed layers from the model without filter has a better agreement to the experimental data. Application of numerical filter to these layers reduces the Pearson correlation and increases the value RMSE, especially for the top layer.

Table 3 Filter Evaluation (WaveFront Location)

Case	With Filter (m)	Without Filter (m)	Experiment (m)
1	2.22	2.32	2.42
2	2.02	2.20	2.45

A comparison of the wavefront location from the experiment, model with filter, and without a filter, is given in Table 3. In general, the estimated location of the wavefront is behind the experiment data. It was found that the model without filter performs better in predicting the location of the wavefront. The movable bed around the wavefront is highly affected by the free surface. Therefore, a more accurate wavefront location will provide a better estimation of the top layer and bed layer profiles. However, it should be noted that oscillation and numerical instability around the wavefront are very high. Application of the numerical filter significantly reduces oscillation and therefore, the overall prediction of the free surface is better.

6. CONCLUSIONS

A Taylor Galerkin model for movable bed dam break flows has been developed. The model was successfully used to simulate an experimental case. The free surface profile, the top layer profile, and the bed layer profile show a good comparison between those obtained from the model to those obtained from the experiment.

The developed model employs a numerical filter to handle the shock. The numerical filter significantly reduces the oscillation due to the numerical instability. The applied filter successfully increases the model accuracy in predicting the free surface profiler. However, its application leads to a less accurate wavefront and movable bed estimation.

Application of filter requires further study. The developed model can be further upgraded by improving the filter with those based on other methods such as the slope limiter function, with consideration of movable bed. Other application possibilities of the developed model could be more realistic conditions, regarding various flow directions. These include bed load transport near the threshold of motion, the transition to debris flows, and fine sediments instead of coarse grains transport problems.

7. ACKNOWLEDGMENTS

This work is supported by the Faculty of Civil and Environmental Engineering, ITB through The Program of Research, Community Service, and Innovation for Research Division ITB (P3MI ITB), the year 2018.

8. REFERENCES

[1] Yakti B.P., Adityawan M.B., Farid M., Suryadi Y., Nugroho J., and Hadihardaja I.K., 2D Modeling of Flood Propagation due to the Failure of Way Ela Natural Dam, MATEC Web of Conferences 147, 03009, 2018

[2] Peng S.H., 1D and 2D Numerical Modeling for Solving Dam-Break Flow Problems Using Finite Volume Method, Journal of Applied Mathematics, Article ID 489269, 14 pages, 2012.

[3] Farid M., Yakti B.P., Rizaldi A., Adityawan M. B., Finite Difference Numerical Scheme for Simulating Dam Break Flow, The 5th HATHI International Seminar on Water Resilience in a Changing World, 2016

[4] Bellos V., and Hrissanthou V., Numerical Simulation of a Dam-Break Flood Wave, European Water, 33: 45-53, 2011.

[5] Adityawan M.B., Tanaka H., and Lin P.Z., Boundary Layer Approach In The Modeling Of Breaking Solitary Wave Runup, Coastal Engineering 06(03):167–177, 2013.

[6] Adityawan M.B. and Tanaka H., Dam break wave simulation using the simultaneous coupling method, Proceedings of 34th IAHR Congress, 2013.

[7] Comblen R., Legrand S., Deleersnijder E., and Legat V., A Finite Element Method for Solving The Shallow Water Equations on The Sphere, Ocean Modelling, Volume 28 (1-3), pp. 12-23, 2009.

[8] Ortiz P., Shallow Water Flows Over Flooding Areas by a Flux-Corrected Finite Element Method, Journal of Hydraulics Research 52:241–252, 2014.

[9] Antonopoulos D.C., and Dougalis V.A., Galerkin-finite element methods for the shallow water equations with characteristic boundary conditions, IMA Journal of Numerical Analysis, Volume 37, Issue 1, pp. 266–295, 2017.

[10] Spinewine B. and Capart H., Intense bed-load due to a sudden dam-break, Journal of Fluid Mechanics, Vol. 731, 2013, pp.579-614.

[11] Spinewine B. and Zech Y., Small-Scale Laboratory Dam-Break Waves on Movable Beds, Journal Hydraulics Research, Vol 45, 2007, pp. 73-86.
[12] Fracarollo L., Capart H., and Zech Y., A Godunov Method for The Computation of Erosional Shallow Water Transients, International Journal for Numerical Methods in Fluids, Vol.41, 2003, pp. 951-976.
[13] Fraccarollo L. and Capart H., Riemann Wave Description of Erosional Dam-Break Flows, Journal Fluid Mechanics, Vol. 461, 2002, pp. 183-228.
[14] Donea J., A Taylor-Galerkin Method fo Convective Transport Problems, International Journal for Numerical Methods in Engineering, Vol. 20, 1984, pp. 101-119.
[15] Zienkiewicx O.C., Peraire J., and Morgan K., Shallow Water Problems: A General Explicit Formulation, International Journal for Numerical Methods in Engineering, Vol. 22, 1986, pp. 547-574.
[16] Harlan D., Transport Phenomena Analysis on Shallow Water Using Taylor Galerkin Finite Element Method, unpublished Master Thesis at ITB, 1998.
[17] Natakusumah D.K., Wijayasari S.I., Harlan D., and Dahana M., A General Finite Element-Flux Corrected Transport Algorithm for Flow and Transport Problems in Shallow Water and Analogous Problems, Proceeding of Seminar on Sediment Transport Modelling, 1999, pp.98-112.
[18] Zendrato N.L.H., Harlan D., Adityawan M.B., and Natakusumah, D.K., 1D Numerical Modelling of Dam Break Using Finite Element Method, Proceedings of The 2nd Conference for Civil Engineering Research Network, 2018.
[19] Hansen W., Hydrodynamical methods applied to oceanographic problems, Proc. Symp. Math.-hydrodyn. Meth. Phys. Oceanogr., 1962.
[20] Adityawan M.B. and Tanaka H., Bed Stress Assessment under Solitary Wave Run-Up, Earth Planets Space, Vol 64, 2012, pp.945-954.